24th INTERNATIONAL CONGRESS ON SOUND AND VIBRATION
23–27 July 2017, London

ICSV24
23-27JULY 2017
LONDON CALLING

FREQUENCY DOMAIN PREDICTIONS OF THE ACOUSTIC REFLECTION COEFFICIENT OF A COMBUSTOR EXIT NOZZLE WITH LINEARIZED NAVIER-STOKES EQUATIONS

Max Zahn
Technical University of Munich, Chair of Thermodynamics, Munich, Germany
email: max.zahn@tum.de

Moritz Schulze

Michael Wagner

Christoph Hirsch

Thomas Sattelmayer
Technical University of Munich, Chair of Thermodynamics, Munich, Germany

In this investigation the acoustic reflection properties of a combustor exit nozzle is characterized based on a coupled Computational Fluid Dynamics/Computational Aeroacoustic (CFD/CAA) methodology. This hybrid approach utilizes a stabilized Finite-Element method to solve the Linearized Navier-Stokes Equation (LNSE) in frequency space on the basis of a Reynolds Averaged Navier-Stokes (RANS) mean flow state. First numerical results are validated against measurements for different Mach numbers in the nozzle throat at ambient conditions. In this regard, the reflection coefficient of the exit nozzle is determined in an impedance test rig at ambient temperature. The resulting reflection coefficients are also verified against an analytical approach. Subsequently, the RANS/LNSE-approach is used to predict the acoustic properties at combustion conditions, considering exhaust gas temperatures of 1500K and various nozzle throat Mach numbers. The effect of the nozzle-throat Mach number on the predicted reflection coefficient amplitudes of the exit nozzle is demonstrated and acoustic loss mechanisms are discussed.
Keywords: gas turbines, aero-acoustics, Linearized Navier-Stokes Equations, Finite Element Method

1. Introduction

A major concern in modern industrial gas turbines is the occurrence of combustion instabilities. The prediction of such self-sustained oscillations in the stage of design requires an accurate acoustic characterization of all combustor components. The focus of this study is to investigate the acoustic properties of the combustor exit where exhaust gas is accelerated to high Mach numbers in the first turbine stage. At full load the turbine inlet is usually choked, in consequence the acoustic system is decoupled from the surrounding. In case of part load however choked conditions are often not reached, which changes the acoustic boundary conditions of the turbine inlet. The exit of the combustion chamber has therefore substantial impact on combustion dynamics (see Bothien [1]) as the acoustic properties of the combustor exit considerably depend on the Mach number in the turbine stage. To obtain such conditions in case of lab-scale combustor experiments, exit nozzles are often used instead, e.g., in [2].

In the sequel the experimental and analytical acoustic charaterization of an investigated combustor exit nozzle is presented as well as the used numerical procedure for predicting acoustic properties, which is based on a coupled RANS/LNSE methodology. The evaluated reflection coefficients obtained by means of the different approaches are then compared for ambient temperatures and different nozzle throat Mach numbers. Occurring acoustic loss mechansims are identified and discussed. The RANS/LNSE methodology is finally applied to estimate the acoustic reflection properties for combustion conditions and various nozzle throat Mach numbers.

2. Acoustic Characterization of Exit Nozzle

2.1 Exit Nozzle Design

The investigated exit nozzle is formed by a circular entry plane with an outer diameter of 70mm and an inner diameter of 60.1mm, cf. Fig.1. In flow direction it is followed by a quarter circle transition with radius r=18.5mm, which converges to the nozzle throat diameter of d=23.1mm. The length of the nozzle throat is 52.5mm.

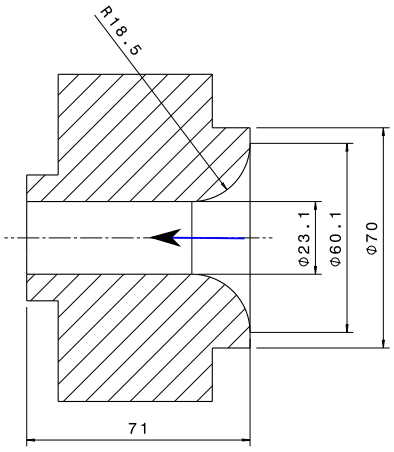

Figure 1: Exit nozzle design.

2.2 Experimental, Analytical and Numerical Acoustic Characterization of Exit Nozzle

Experimental Investigations

For the experimental determination of the acoustic reflection properties, the investigated exit nozzle is mounted coaxially to an impedance tube test rig to obtain the characteristic reflection coefficient at ambient conditions (1013mbar, 295K). The experimental setup is illustrated and described in [3]. Continuous siren forcing is used for an acoustic excitation. The frequency of the siren is varied and the pressure signals are recorded for each frequency step. Assuming planar wave propagation in the impedance duct the pressure data are decomposed into the one dimensional downstream propagating wave $\hat{f}$ in the impedance tube and the upstream propagating wave $\hat{g}$, hence referred to as Riemann invariants. $\hat{f}$ and $\hat{g}$ are reconstructed from the measured pressure-fluctuation data with the Multi-Microphone Method [4] and are complex-valued, indicated by $\hat{\cdot}$ - quantity. The reconstructed field for each frequency is finally extrapolated to the end of the impedance tube where the exit nozzle is mounted. From the data the complex reflection coefficient R,

$$R = \frac{\hat{g}}{\hat{f}}, \tag{1}$$

is determined as a function of frequency.

Analytical Reflection Coefficient Determination

The acoustic characterization of the nozzle can be thought of as a twofold problem, cf.[5]. On the one hand the nozzle acoustically represents a continuous area contraction generally without flow separation in case of a steady flow exiting the nozzle. On the other hand the exit of the nozzle describes an open end boundary.

Marbel and Candel [6] derived an analytical expression for the reflection coefficient of a continuous area contraction where a mean flow is accelerated. This approach assumes a compact nozzle for the evaluation of the reflection coefficient. Compactness holds when the acoustic wavelength is much longer in comparison to the characteristic length of the nozzle. Thus the nozzle can be regarded as a discontinuity for acoustic wave propagation. The analytical solution of [6] for an adiabatic, loss-free (no vortex shedding), compact nozzle considers the Mach number M_1 before the acceleration of the flow and M_2 after the acceleration of the flow. For neglected entropy waves the analytical solution of the reflection coefficient for a choked compact nozzles ($M = 1$) reads as

$$R = \frac{1 - 0.5(\gamma - 1)}{1 + 0.5(\gamma - 1)}. \tag{2}$$

This reflection coefficient has no dependency on M_2 since no information can propagate from downstream to upstream for choked conditions. Lamarque and Poinsot extended in [7] the analytical solution of [6] for subsonic flow conditions and under consideration of an open-end boundary (R=-1) at the nozzle exit, reading as

$$R = \frac{M_1 + 1}{M_1 - 1} \frac{(M_1 - M_2)(M_2 + 1)(1 - 0.5(\gamma - 1)M_1M_2) + (M_1 + M_2)(M_2 - 1)(1 + 0.5(\gamma - 1)M_1M_2)}{(M_1 + M_2)(M_2 + 1)(1 + 0.5(\gamma - 1)M_1M_2) + (M_1 - M_2)(M_2 - 1)(1 - 0.5(\gamma - 1)M_1M_2)}. \tag{3}$$

Due to the compactness assumption, Eq.(2) and Eq.(3) are only real-valued and the phase is always zero because no energy is stored. This implies however that the expressions are limited to low frequencies. Advanced analytical methods, e.g., by [8], [9] and recently [10] also consider non-compact nozzles. Still the crucial boundary conditions downstream of the area contraction have to be provided for unchoked flow conditions to evaluate the reflection properties upstream of the nozzle.

Numerical Procedure and Variational Formulation of the LNSE and Galerkin Approximation

A coupled Computational Fluid Dynamics/ Computational Aeroacoustic (CFD/CAA) methodology as it is presented, e.g., in [11]-[14] and [3], is applied to characterize the acoustic reflection properties of the exit nozzle numerically and gain insight into the physical mechanisms that induce losses of acoustic energy. In this hybrid approach the fluid dynamic field is computed with the finite-volume solver ANSYS CFX by using a SST Reynolds Averaged Navier-Stokes (RANS) model. Based on the resulting CFD mean flow state, a stabilized Finite-Element method solves the Linearized Navier-Stokes Equation (LNSE) in frequency space. The considered two-dimensional computational domain is shown in Fig.2. It comprises a section of the impedance tube and adjacent parts of the surrounding.

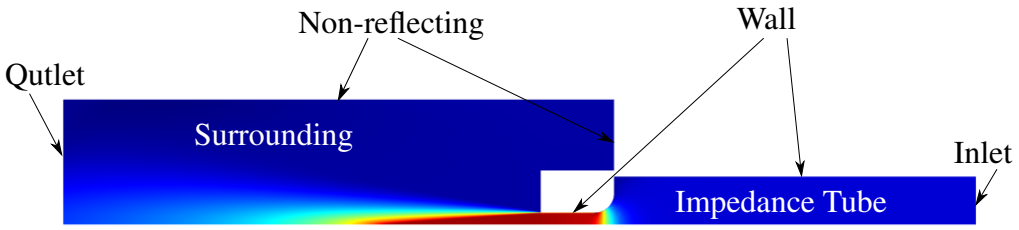

Figure 2: Computational domain with boundaries.

The isentropic LNSE in form of mass and momentum equations are considered, which can formally be described with regard to functional analysis using mathematical operators $\mathcal{L}$, (see, e.g., Zahn et al. [14]): $\mathcal{L}_{\hat{\rho}}\mathbf{\Phi} = 0$, $\mathcal{L}_{\hat{v}}\mathbf{\Phi} = 0$.
Here $\mathbf{\Phi}$ denotes the vector $\mathbf{\Phi} = (\hat{\rho}, \hat{\boldsymbol{v}})^T$, with the complex-valued density $\hat{\rho}$ and the complex-valued velocity vector $\hat{\boldsymbol{v}}$.

The corresponding weak form of the LNSE with appropriate solution function spaces $\mathcal{S}_{\hat{v}}$, $\mathcal{S}_{\hat{\rho}}$ for $\hat{\boldsymbol{v}}$, $\hat{\rho}$ and weighting function spaces $\mathcal{S}_{w_{\hat{v}}}$, $\mathcal{S}_{w_{\hat{\rho}}}$ for the weighting functions $\boldsymbol{w}_{\hat{\boldsymbol{v}}}$, $w_{\hat{\rho}}$, respectively, reads as: find $\hat{\rho} \in \mathcal{S}_{\hat{\rho}}$ and $\hat{\boldsymbol{v}} \in \mathcal{S}_{\hat{v}}$ such that

$$(w_{\hat{\rho}}, \mathcal{L}_{\hat{\rho}}\mathbf{\Phi}) = 0 \quad \forall w_{\hat{\rho}} \in \mathcal{S}_{w_{\hat{\rho}}}, \tag{4}$$

$$(\boldsymbol{w}_{\hat{v}}, \mathcal{L}_{\hat{v}}\mathbf{\Phi}) = 0 \quad \forall \boldsymbol{w}_{\hat{v}} \in \mathcal{S}_{w_{\hat{v}}}, \tag{5}$$

where $(\cdot, \cdot)$ is the L_2-inner product.

With regard to a Galerkin finite-element approximation, $\hat{\rho}$ and $\hat{\boldsymbol{v}}$ are approximated element-wise ($\hat{\rho}^h \in \mathcal{S}^h_{\hat{\rho}}$ & $\hat{\boldsymbol{v}}^h \in \mathcal{S}^h_{\hat{v}}$). The corresponding function spaces $\mathcal{S}^h$ are replaced subspaces $\mathcal{S}^h \subset \mathcal{S}$ with local support on the "finite elements" (characteristic length scale h) of the discretized domain Ω. Thus a discrete variational finite-element formulation of the LNSE is obtained: find $\hat{\rho}^h \in \mathcal{S}^h_{\hat{\rho}}$ and $\hat{\boldsymbol{v}}^h \in \mathcal{S}^h_{\hat{v}}$ such that

$$\underbrace{\int_{\Omega^e} \mathcal{L}_{\hat{\rho}}\mathbf{\Phi}^h w^h_{\hat{\rho}} \quad d\Omega^e}_{\text{Standard FEM}} + \underbrace{\int_{\Omega^e} \tau_{\hat{\rho}}(\mathcal{L}_{\hat{\rho}} w^h_{\hat{\rho}})(\mathcal{L}_{\hat{\rho}}\mathbf{\Phi}^h) \quad d\Omega^e}_{\text{GLS term}} = \mathcal{R}_{\hat{\rho}} \qquad \forall w^h_{\hat{\rho}} \in \mathcal{S}_{w_{\hat{\rho}}}, \tag{6}$$

$$\underbrace{\int_{\Omega^e} \mathcal{L}_{\hat{v}}\mathbf{\Phi}^h w^h_{\hat{v}} \quad d\Omega^e}_{\text{Standard FEM}} + \underbrace{\int_{\Omega^e} \tau_{\hat{v}}(\mathcal{L}_{\hat{v}} w^h_{\hat{v}})(\mathcal{L}_{\hat{v}}\mathbf{\Phi}^h) \quad d\Omega^e}_{\text{GLS term}} = \mathcal{R}_{\hat{v}} \qquad \forall w^h_{\hat{v}} \in \mathcal{S}_{w_{\hat{v}}}. \tag{7}$$

To prevent oscillating solutions for convection dominated cases, a Galerkin/least-squares (GLS) stabilization is supplemented in Eq.(6), (7) to obtain a stabilized method, with the stabilization parameter $\tau_{\hat{\tau}} = \tau_{\hat{v}} = max\left(\frac{\alpha h}{\bar{v}+c}\right)$ being the only empirical coefficient. In this analysis α is set accordingly to previous studies with the RANS/LNSE methodology, cf.[12]. $\mathcal{R}$ denote the residuals.

Simulation Model

Non-reflecting boundary conditions are imposed at the inlet, outlet and surrounding for this investigation. In this context, an impedance Z is prescribed in each case yielding $Z = \frac{\hat{p}}{\hat{\mathbf{v}}\mathbf{n}\bar{\rho}c} = 1$. Here $\mathbf{n}$ is the surface normal vector. Furthermore, it is assumed that acoustic boundary layers are negligible, thus all wall boundary conditions are defined as $\hat{\mathbf{v}} \cdot \mathbf{n} = 0$.

To impose an acoustic forcing in the simulations a piston-like spatially bounded volume source is defined upstream of the exit nozzle in the impedance tube section of the computational domain. This forcing excites plane waves only in axial direction at each frequency step. In accordance to the experiments, pressure-fluctuation signals are extracted at probes located upstream of the exit nozzle. $\hat{f}$ and $\hat{g}$ are subsequently reconstructed from the pressure data with the Multi-Microphone Method [4] and the reflection coefficient $R = \frac{\hat{g}}{\hat{f}}$ is evaluated. The computations are performed on a two-dimensional unstructured grid consisting of approx. 40000 linear tetrahedral elements. MUMPS (Multifrontal Massively Parallel Sparse) direct solver is used for solving the discrete variational finite-elements formulation of the LNSE in frequency domain.

2.3 Results and Discussion of Acoustic Energy Loss Mechanisms

The resulting amplitudes $|R|$ and phases $\phi(R)$ of the exit nozzle reflection coefficients determined by the RANS/LNSE-approach and experiments (Exp.) are compared for different throat Mach numbers $M \approx 0,\ M = 0.2,\ M = 0.4,\ M = 0.6,\ M = 0.8,\ M = 1$ in Fig.3 (left column) at ambient

Figure 3: Resulting acoustic reflection coefficients obtained experimentally, numerically and analytically at different Mach numbers for cold (left) and combustion conditions (right).

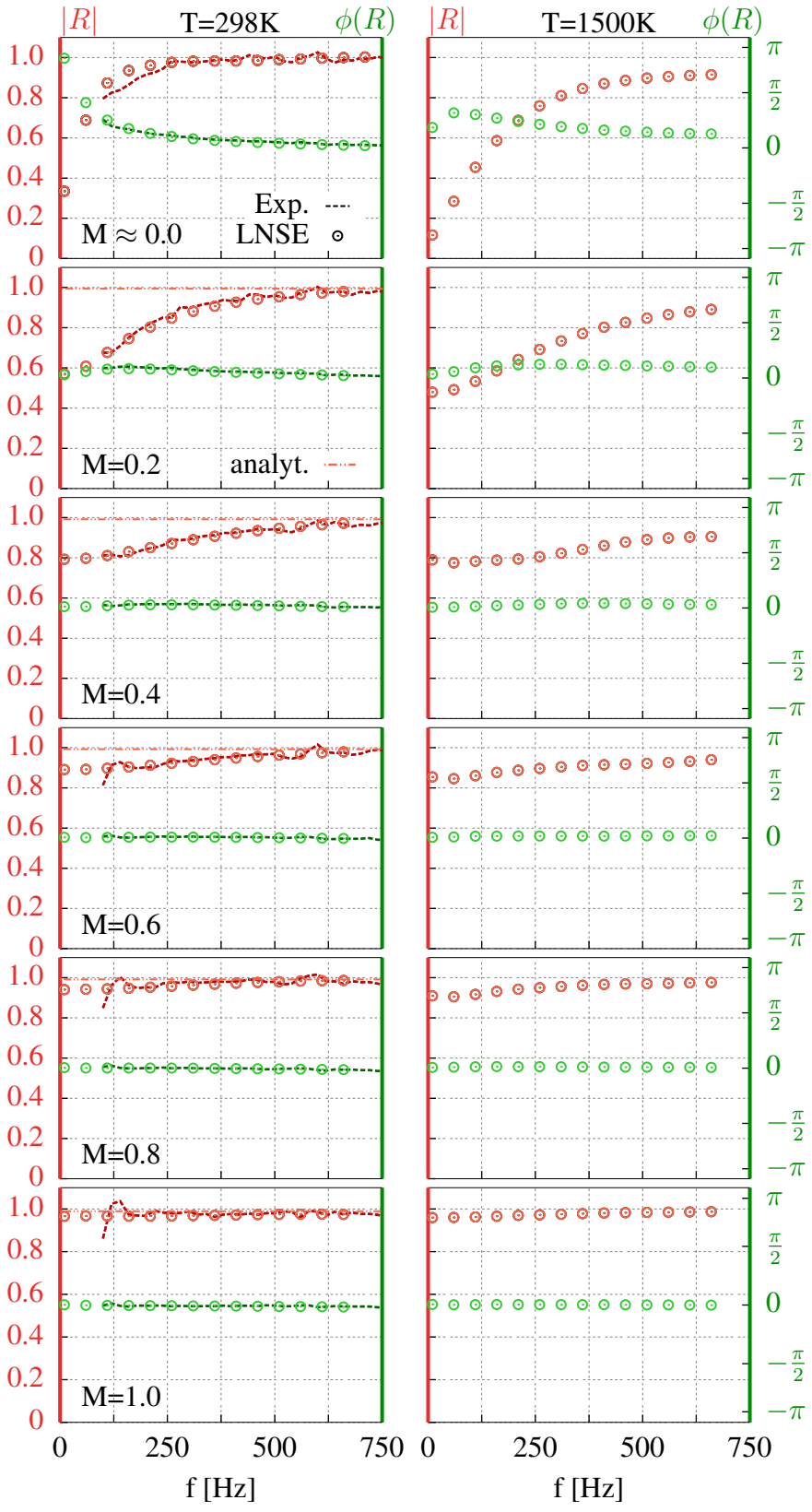

temperature. It is demonstrated that the results of the RANS/LNSE-procedure compare very well to the experimentally determined data for all investigated Mach numbers in the considered frequency range. The analytical expressions defined in Eq.(2) and Eq.(3) are also evaluated in Fig.3 (left column) depending on the corresponding Mach numbers M_1 upstream of the nozzle entry and M_2 in the throat, which is plotted in Fig.3, indicated by (analyt.). It can be observed that the exit nozzle, under consideration of an open-end boundary condition at the exit, behaves in this regard nearly like a rigid wall (R=1) for all flow conditions.

The acoustic properties resulting for $M = 1$ in the nozzle throat are considered in more detail first. No information can propagate upstream through the choked throat and thus the nozzle is decoupled from the exit and the surrounding. For these conditions the numerical and experimental results are in good accordance with the analytical solution of [6]. For a smaller Mach number of $M = 0.8$ the analytical expression for subsonic conditions (Eq.(3)) is still in sufficient agreement with the numerical and experimental results. With further decreasing Mach numbers however significant deviations between the analytical expression and the numerical/experimental results arise especially in the low frequency range. It can be seen in Fig.3 (left) that the reflection coefficients exhibit distinct sound absorption particularly occurring at low frequencies and most significantly for low Mach numbers. Also a considerable phase offset is observed for low Mach number, which decreases with rising Mach number.

For Mach numbers in the throat distinctively smaller than one, the nozzle is no longer decoupled from the exit and the surrounding, as already emphasized. Thus the acoustic properties of the exit gains importance because it can affect the acoustics upstream, which is not captured by the analytical expression (Eq.(3)). To get a better understanding of the observed low frequency characteristics, the exit of the nozzle is investigated in more detail. An "open end" boundary such as a hugh area expansion without background flow is discussed first with respect to linear acoustics. This exhibits a distinct jump in impedance at the nozzle throat exit, which can be represented by a pressure release condition $R = -1$ as indicated above, (consult also, e.g., [15]). Hence, the acoustic flux of an incident wave is completely reflected and non is transferred. This simplification however is only valid for small frequencies. For higher frequencies also sound radiation or transmission of sound at the "open end", respectively, has to be accounted for as summarized, e.g., in [16]. Nevertheless, this cannot explain the observed sound absorption for low frequencies.

It was shown in [14] in context of an acoustic swirl-burner characterization that acoustic mode coupling, particularly the transfer of acoustic energy into fluctuating vortical modes in regions of flow inhomogeneities evoke essential acoustic absorption. Coupling regions were localized at edges of area expansions and within shear layers where strong mean vorticity is present. With regard to the mean flow jet that is separating at the nozzle exit and with evolving shear layers downstream, comparable mode coupling regions are existing. Especially strong mean vorticity is produced right at the abrupt area expansion where the mean flow is exiting the nozzle throat, resulting in a turbulent separation area. Hence acoustic perturbations, which encounter the nozzle exit plane, couple with these flow inhomogeneities at the area expansion lip and produce fluctuating vortical structures. The fluctuating vorticity gets subsequently convected with the mean flow and is amplified further downstream before being dissipated again. This can be observed in Fig.4, which shows the normalized field of velocity fluctuations resulting from the RANS/LNSE simulations. The computed velocity field consists of acoustic as well as vortical velocity disturbances with distinguishing propagation properties. Acoustic fluctuations propagate with the speed of sound, fluctuating vortical structures are transported convectively by the mean flow. In Fig.4 vortical structures assessed by their short wave length emerge in the shear layers of the mean jet, which are indicated by mean velocity contour lines (black). These vortices originate from the edge of the area expansion where they are formed due to mode coupling. Hence this causes attenuation of acoustic energy that is not reflected at the "open end" boundary. The produced fluctuating vortices are then convected by the jet and get further amplified downstream in the jet shear layers before they dissipate.

A probe located in the nozzle throat close to the exit plane (cf. Fig.4) records axial velocity fluctuations. Fig.5 illustrates the resulting magnitude of the velocity fluctuations depending on the frequency. It can be seen that for smaller frequencies axial velocity perturbations gain intensity. Oscillations of higher amplitude cause greater acoustic mode coupling, and thus inducing increased absorption of acoustic energy. Speaking in terms of the acoustic Strouhal number $Str_{ac} = \frac{\omega \cdot d/2}{|v_{ax}|}$ (d as the nozzle diameter), which is also evaluated at the probe location and plotted in Fig.5, a decrease in magnitude occurs with decreasing frequency. Smaller acoustic Strouhal numbers are related to greater acoustic losses as discussed in [16].

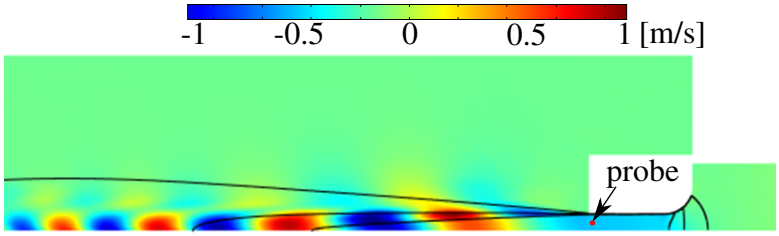

Figure 4: Normalized real-valued acoustic velocity field with mean velocity contour lines (black).

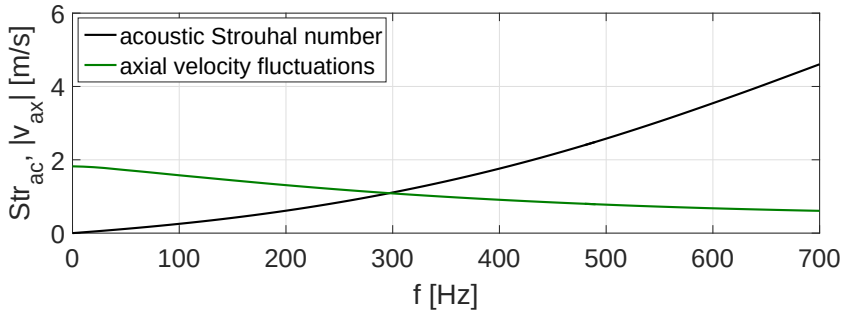

Figure 5: Amplitude of axial velocity fluctuations and acoustic Strouhal number evaluated at probe location.

It was demonstrated that the RANS/LNSE-methodology can capture the acoustic nozzle properties for cold flow conditions precisely. Subsequently, the reflection coefficients of the exit nozzle are predicted for combustion conditions considering exhaust gas temperatures at 1500K and the same throat Mach numbers. The resulting acoustic characteristics are illustrated in Fig.3 (right). The differences between cold flow and combustion conditions are manifested more distinctly for small Mach numbers, convergence arises for higher Mach-numbers. In each case a lower amplitude of the reflection coefficients with respect to cold flow conditions is observed, whereas the corresponding phase shows a greater offset compared to the cold case. For the choked nozzle (M=1) the reflection coefficients are the same for both conditions since the variation of the Mach number upstream of the nozzle is negligible.

3. Conclusion

A coupled Computational Fluid Dynamics/Computational Aeroacoustic (CFD/CAA) methodology is applied that solves the Linearized Navier-Stokes Equation (LNSE) based on a RANS mean flow state. A stabilized Finite-Element framework evaluates the LNSE in frequency space and is used to compute the acoustic reflection properties of a combustor exit nozzle. For ambient temperature and various nozzle throat Mach numbers very good agreement to experimental data could be achieved. The RANS/LNSE methodology is utilized consequently to estimate the characteristic reflection coefficient of the combustor exit nozzle for combustion conditions, considering exhaust gas

temperatures of 1500K and different nozzle throat Mach numbers. The dissipative character of the investigated nozzle properties for low Mach numbers and in the lower frequency range is investigated additionally. An acoustic mode coupling effect at the end of the exit nozzle can be observed in the computed fluctuating velocity fields where the mean flow separates. Acoustic energy is transfered in this regard into fluctuating vortical modes in regions of distinct flow inhomogeneities and thus evoking losses of acoustic energy, which cannot be reflected at the open end (pressure release boundary). The acoustic mode coupling intensity and hence the magnitude of acoustic absorption depends on the acoustic Strouhal number. This quantity is evaluated at the end of the nozzle throat and exhibits a frequency dependency. For lower frequencies the acoustic Strouhal number decreases, which can be related to higher acoustic absorption. The regarded analytical solutions that characterize the reflection coefficient of a continuous area contraction under consideration of an open-end boundary at the exit does not include the described acoustic loss mechanism. In consequence, inaccurate acoustic characteristics are obtained for low frequencies and low Mach numbers.

References

1. Bothien, M., *Impedance Tuning: A Method for Active Control of the Acoustic Boundary Conditions of Combustion Test Rigs*, Ph.D. thesis, Technical University Berlin, (2008).
2. Fanaca, D., *Influence of Burner-Burner Interactions on the Flame Dynamics in an Annular Combustor*, Ph.D. thesis, Technical University Munich, (2010).
3. Zahn, M., Schulze, M., Hirsch, C. and Sattelmayer, T. Impact of quarter wave tube arrangement on damping of azimuthal modes, *Proceedings of ASME Turbo Expo 2016*, no. GT2016-56540, (2016).
4. Munjal, M. L. and Doige, A. G. Theory of a two source-location method for direct experimental evaluation of the four-pole parameters of an aeroacoustic element, *Journal of Sound and Vibration*, **141** (2), 323–333, (1990).
5. Bechert, D. Sound absorption caused by vorticity shedding, demonstrated with a jet flow, *Journal of Sound and Vibration*, **70** (3), (1980).
6. Marble, F. and Candel, S. Acoustic disturbances from gas nonuniformities convected through a nozzle, *Journal of Sound and Vibration*, **55** (2), (1977).
7. Lamarque, N. and Poinsot, T. Boundary conditions for acoustic eigenmodes computation in gas turbine combustion chambers, *AIAA Journal*, **46** (9), (2008).
8. Stow, S., Dowling, A. and Hynes, T. Reflection of circumferential modes in a choked nozzle, *Journal of Fluid Mechanics*, **467**, (2002).
9. Goh, C. and Morgans, A. The effects of entropy wave dissipation and dispersion on thermoacoustic instabilities in a model combustor, *17th AIAA/CEAS*, no. 2914, (2011).
10. Duran, I. and Moreau, S. Solution of the quasi-one-dimensional linearized Euler equations using flow invariants and the Magnus expansion, *Journal of Fluid Mechanics*, **723**, (2013).
11. Schulze, M., Gikadi, J. and Sattelmayer, T. Acoustic Admittance Prediction of two Nozzle Designs of different length using Frequency Domain Simulations, *5th European Conference for Aeronautics and Space Sciences, Munich, Germany*, (1-5 July 2013).
12. Gikadi, J., Föller, S. and Sattelmayer, T. Impact of turbulence on the prediction of linear aeroacoustic interactions: Acoustic response of a turbulent shear layer, *Journal of Sound and Vibration*, **333** (24), 6548–6559, (2014).
13. Gikadi, J., *Prediction of Acoustic Modes in Combustors using Linearized Navier-Stokes Equations in Frequency Space*, Ph.D. thesis, Technical University Munich, Munich, (2013).
14. Zahn, M., Schulze, M., Hirsch, C., Betz, M. and Sattelmayer, T. Frequency Domain Predictions of Acoustic Wave Propagation and Losses in a Swirl Burner with Linearized Navier-Stokes Equations, *Proceedings of ASME Turbo Expo 2015*, Montreal, Canada, June 15-19, no. GT2015-42723, ASME, (2015).
15. Lieuwen, T. C., *Unsteady combustor physics*, Cambridge University Press, New York (2012).
16. Peters, M. C. A. M., Hirschberg, A., Reijnen, A. J. and Wijnands, A. P. J. Damping and reflection coefficient measurements for an open pipe at low Mach and low Helmholtz numbers, *Journal of Fluid Mechanics*, **256** (-1), 499, (1993).